Rhombohedral and tetragonal nanotwin domains and thermally induced phase transformations in PZN–8%PT single crystals

2008 J. Phys.: Condens. Matter 20 445218

(http://iopscience.iop.org/0953-8984/20/44/445218)

J. Phys.: Condens. Matter **20** (2008) 445218 (7pp) doi:10.1088/0953-8984/20/44/445218

Rhombohedral and tetragonal nanotwin domains and thermally induced phase transformations in PZN–8%PT single crystals

W S Chang[1], L C Lim[1], P Yang[2], C-M Hsieh[3] and C-S Tu[3]

[1] Department of Mechanical Engineering, National University of Singapore, 10 Kent Ridge Crescent, 112960, Singapore
[2] Singapore Synchrotron Light Source, National University of Singapore, 5 Research Link, 117603, Singapore
[3] Department of Physics, Fu Jen Catholic University, Taipei, Taiwan 242, Republic of China

E-mail: weisea@nus.edu.sg (W S Chang), mpelimlc@nus.edu.sg, slsyangp@nus.edu.sg and 039611@mail.fju.edu.tw (C-S Tu)

Received 17 July 2008, in final form 13 September 2008
Published 10 October 2008
Online at stacks.iop.org/JPhysCM/20/445218

Abstract

Phase transformations of unpoled (annealed) and annealed-and-poled $0.92Pb(Zn_{1/3}Nb_{2/3})O_3$–$0.08PbTiO_3$ (PZN–8%PT) single crystals have been examined by combined bulk property characterization and high-resolution x-ray diffraction studies. The results show that at room temperature both unpoled and poled PZN–8%PT single crystals are in the rhombohedral state with a mixture of microscopic (R) and nanotwin (R_{NT}) domains. Both crystals undergo a $R(+R_{NT}) - T(+T_{NT}) - C$ transformation sequence upon zero-field heating (ZFH), where T and C denote the tetragonal and cubic phases, respectively, and T_{NT} is a brief tetragonal nanotwin state.

(Some figures in this article are in colour only in the electronic version)

1. Introduction

The high piezoelectric coefficients of $d_{33} > 1500$ pC N^{-1}, high electromechanical coupling of $k_{33} > 90\%$, and strain levels of $>1.7\%$ exhibited by relaxor-based ferroelectric $(1-x)Pb(Zn_{1/3}Nb_{2/3})O_3$–$xPbTiO_3$ (PZN–xPT) and $(1-y)Pb(Mg_{1/3}Nb_{2/3})O_3$–$yPbTiO_3$ (PMN–yPT) solid-solution single crystals [1] have made them candidate materials for future high-performance sensors and actuators. Earlier studies have shown that the excellent properties may be attributed to the presence of monoclinic phases (i.e. M_A- and M_B-type space group *Cm*, and M_C-type space group *Pm*) and orthorhombic O (space group of *Amm2*) phase, which act as the structural bridges in the various phase transformations [2–10]. Despite the above, the existence of these low-symmetry phases remains under much debate. For instance, it has been argued that the reported monoclinic phases may in fact be a strained or distorted R phase instead [11]. On the other hand, adaptive phase models and diffraction theories, proposed by Viehland and co-workers [12, 13] and Wang [14, 15], respectively, suggest that the observed monoclinic diffractions may in fact be those of nanotwin domains. Experimental support for the presence of nanodomains was obtained by Bdikin *et al* [16]. More recently, the nanotwin domains were reported in both the PZN–PT [17, 18] and PMN–PT [19] single crystals.

This work aims at examining the transformation sequences in both unpoled (i.e. annealed) and annealed-and-poled PZN–8%PT single crystals upon heating, by combining bulk property characterization and high-resolution diffraction studies. Although the phase transformational sequence of bulk PZN–8%PT single crystal has been studied by Ohwada *et al* [20], the situation was compounded by the different prehistories (electrical and/or thermal) that the reported sample had experienced. The prehistories could have influenced the resultant domain structures of the test sample as reported by Uesu *et al* [21]. In this study, annealed PZN–8%PT samples

taken from the same wafer with no prehistory of electric (E) field application were used as the starting material.

2. Experimental procedure

PZN–8%PT single crystal grown by an improved flux technique [22] was oriented by means of the Laue back-reflection method. The crystal was sliced into specimens of $[100]^L \times [010]^W \times [001]^T$ in orientation and two different dimensions of $3^L \times 1.5^W \times 7^T$ mm^3 and $7^L \times 3^W \times 1.5^T$ mm^3, respectively. All directions are referred to the pseudocubic coordinates. All the samples were annealed at 257 °C for 1 h before any measurements.

The $7^L \times 3^W \times 1.5^T$ mm^3 samples were used for dielectric measurements. They were gold electroded onto the opposite $7^L \times 3^W$ faces by dc sputtering. A Wayne–Kerr analyzer PMA3260A was used to obtain the real parts of dielectric permittivity, ε'. For the unpoled sample, the zero-field heating (ZFH) process was used, in which the data were taken upon heating without any applied E field at a heating rate of 1.5 °C min^{-1}. For the poled sample, prior poling was performed at room temperature with a dc E field $=$ 0.5 kV mm^{-1} along the [001] thickness direction. The poled sample was subsequently tested under ZFH conditions at a heating rate of 1.5 °C min^{-1}. ZFH current density measurements were performed on both the unpoled and poled samples by using a Keithley 6517A electrometer at the same heating rate.

The $3^L \times 1.5^W \times 7^T$ mm^3 samples were used for the HR-XRD studies. Both the unpoled and poled samples were first fractured along the (001) plane to expose the strain-free bulk material. All the HR-XRD measurements were taken from the (001) fractured surfaces only. This was to avoid undesired surface effects produced by mechanical polishing [23, 24].

The HR-XRD study was performed at the Singapore Synchrotron Light Source (SSLS). The diffractometer used was a Huber four-circle system 90000-0216/0 with high-precision 0.0001° step size for omega (ω) and two-theta (2θ) circles. The distance from the entrance slit (S_1) to the sample centre was 688 mm and that from the sample centre to the detector slit (S_4) was 680 mm (adjustable). The storage ring, Helios 2, runs at 700 MeV, which produces a stored electron beam current of 300 mA. The x-ray beam was conditioned to select photon energy by a Si(111) channel-cut monochromator. It was blocked to 0.30 mm in the vertical direction and 3.50 mm in the horizontal direction by the collimating mirror and the slit system (S_1 and S_4) for reciprocal space mapping. The set-up yielded an x-ray beam of about 0.01° in divergence at 8.048 keV. A series of rocking ($\Delta\omega$) scans at a range of 2θ were carried out to form the (002) reciprocal space mapping. A typical step size of 0.03° and typical counting time of 0.5 s for every rotating step were used. No crystal analyser was used. When higher resolution of the diffractions was required, such as when we sought to resolve suspected convoluted diffractions, the vertical slits (S_1 and S_4) were reduced to 0.10 mm and the step size was decreased to 0.005°. Angular resolution better than 0.007° can be achieved with the latter arrangement.

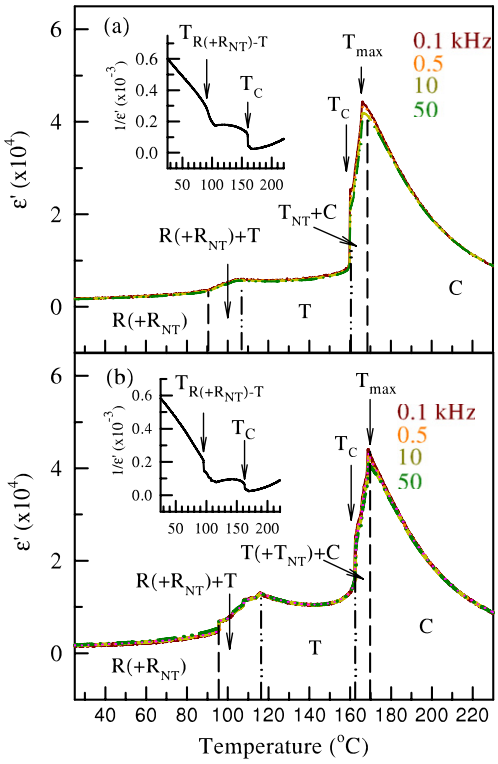

Figure 1. Temperature-dependent dielectric permittivity (ε') curves of (a) unpoled (annealed) and (b) annealed-and-poled PZN–8%PT single crystals under the ZFH process. The inset shows the corresponding $1/\varepsilon'$ versus temperature plot. Sample thickness is 1.5 mm.

3. Results

3.1. Dielectric permittivity measurements

Figure 1(a) shows the temperature- and frequency-dependent dielectric permittivity, ε' of the unpoled (annealed) PZN–8%PT sample. The ε' increased gradually with temperature initially, followed by a weak anomaly over the temperature range of about 90–105 °C. This anomaly can be more readily seen in the $1/\varepsilon'$ versus temperature plot. As shown in the inset of figure 1(a), the value of $1/\varepsilon'$ showed a steeper drop at about 90 °C. In addition, a clear anomaly in ε' (and a step-like decrease in $1/\varepsilon'$) was observed over the temperature range of 160 − 173 °C. The latter anomaly was followed by a frequency-dependent dielectric permittivity maximum (at T_{max}), which may be attributed to the dynamic relaxation processes of polar nanoclusters in the material [25, 26].

Figure 1(b) shows the dielectric spectra of a PZN–8%PT sample after it was poled to 0.5 kV mm^{-1} at room temperature. Two dielectric anomalies, at ≈95 °C and ≈170 °C (T_{max}) respectively, were again observed. These anomalies can be more readily seen in the $1/\varepsilon'$ versus temperature plot (see inset), which shows a step-like drop in $1/\varepsilon'$ in both cases.

3.2. Thermal current density measurements

Figure 2(a) shows the current signals of the unpoled PZN–8%PT single crystal as a function of temperature. The unpoled

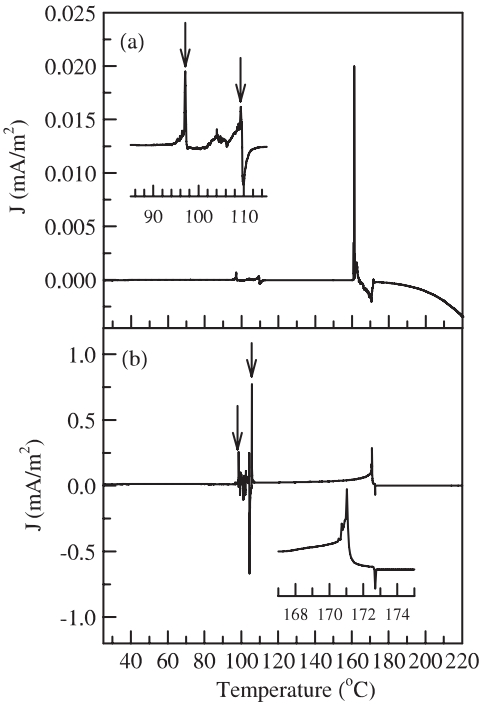

Figure 2. Thermal current density (J) of (a) unpoled (annealed) and (b) annealed-and-poled PZN–8%PT single crystals under the ZFH process. Sample thickness is 1.5 mm.

sample displayed multiple but very weak current signals over the temperature range of 90–113 °C. Of these activities, three more obvious current signals could be noted, at 97 °C, 104 °C and 110 °C, respectively (see inset). There followed a period of no current activities on further heating until about 165 °C, at which a stronger current signal was detected, followed by a string of weak current activities spreading over the temperature range of 165–170 °C.

The current density measurements obtained from the poled sample are given in figure 2(b). Two main groups of current activities could be noted. The first group occurs over the temperature range of 95–107 °C. Multiple but much stronger current signals were noted over the said temperature range, being at least two orders of magnitude higher than the unpoled sample, which culminated with a very strong current signal at about 105 °C. Similar to the unpoled sample, no current activities were detected on further heating until about 165 °C. A stronger current signal was again detected at 170 °C.

3.3. HR-XRD reciprocal space mappings

3.3.1. Unpoled (annealed) PZN–8%PT. To check for possible accompanied phase transformations, several bulk samples prepared from the same crystal were x-rayed. It has to be pointed out that reciprocal space mappings shown below were all taken from the fractured surfaces. This was to expose the stress-free internal structure for the HR-XRD study, so as to avoid possible complications associated with the polished surface layer [23, 24]. Only the (002) HR-XRD reciprocal space mappings as a function of temperature were performed in the present work. The results are shown in figure 3, of which the intensity contours are on a log scale.

Figure 3(a) shows a typical (002) mapping of an unpoled PZN–8%PT single crystal taken at 25 °C. Five diffraction peaks, marked d_1–d_5 in the figure, were detected. These five diffraction peaks are located at three different Bragg angles i.e. d_1 and d_2 at $2\theta \approx 44.95°$ (with $\Delta\omega \approx 0.54°$), d_3 at $2\theta \approx 44.68°$ ($\Delta\omega \approx 0°$), and d_4 and d_5 at $2\theta \approx 44.60°$ ($\Delta\omega \approx 0.24°$). All the peaks except d_3 lie out of the $\omega = 0°$ plane. The diffraction pattern shown in figure 3(a) may arise from one of the following two plausible sources; i.e. from rhombohedral nanotwin (R_{NT}) domains as proposed by Wang [14, 15] or from the existence of a phase mixture. We shall discuss this in more detail later. For the time being, we may assign the room temperature phase of the unpoled PZN–8%PT as the 'low-temperature' phase(s) or 'LT' phase(s) for short.

The room temperature (002) diffraction patterns of the unpoled PZN–8%PT sample remained relatively unaffected as the temperature was increased from 25 °C to about 78 °C. At 80 °C (figure 3(b)), two new peaks superimposing onto the existing diffraction peaks were noted on the (002) mapping, indicating the emergence of a new phase. With increasing temperature, the peaks gradually shifted towards the $\omega = 0°$ plane. At 95 °C (figure 3(c)), only two peaks at $2\theta \approx 44.37°$ and $2\theta \approx 44.86°$ remained. Since both peaks lie in the $\omega = 0°$ plane, the new phase is identified as the T phase. Both the LT and T phases coexisted over the temperature range of 80–95 °C (figures 3(b) and (c)) while only the T phase persisted above 95 °C, which remained the only phase detected up to 160 °C (figures 3(d)–(g)).

Careful observation shows that the C phase, at $2\theta \approx 44.60°$, started to emerge at 160 °C (figure 3(g)). It is interesting to note from figures 3(g) and (h) that the emergence of the C phase caused the diffractions of the T phase to become increasingly tilted out of the $\omega = 0°$ plane. The C phase, at $2\theta \approx 44.66°$, remained the dominant phase above 173 °C (figure 3(i)).

The above experiment was repeated with several other unpoled PZN–8%PT single crystal samples. Similar results were obtained. However, slight variations in the HR-XRD patterns were also noted in a few samples. Figure 4 shows the (002) mappings taken from another unpoled PZN–8%PT sample. This sample exhibited a predominately R structure at room temperature as manifested by the characteristic single broad diffraction peak at $2\theta \approx 44.65°$ (figure 4(a)). There appeared to be a degenerated peak at $2\theta \approx 45.05°$ although its presence remained ambiguous. With increasing temperature, the R peak remained the major peak and the degenerated peak at $2\theta \approx 45.05°$ also became obvious. Figure 4(b) taken at 90 °C shows unbalanced degenerated peaks located at $2\theta \approx 45°$ ($\Delta\omega \approx 0.18°$) in addition to the main R peak at $2\theta \approx 44.65°$. At 95 °C, in addition to the various peaks described above, new diffraction peaks characteristic of the T phase finally emerged despite having a tilted appearance (figure 4(c)). We shall discuss these interesting results later.

3.3.2. Annealed-and-poled PZN–8%PT single crystal. A similar fracture procedure was used to prepare the poled sample for the HR-XRD study except that the sample was given a prior poling treatment at room temperature with an

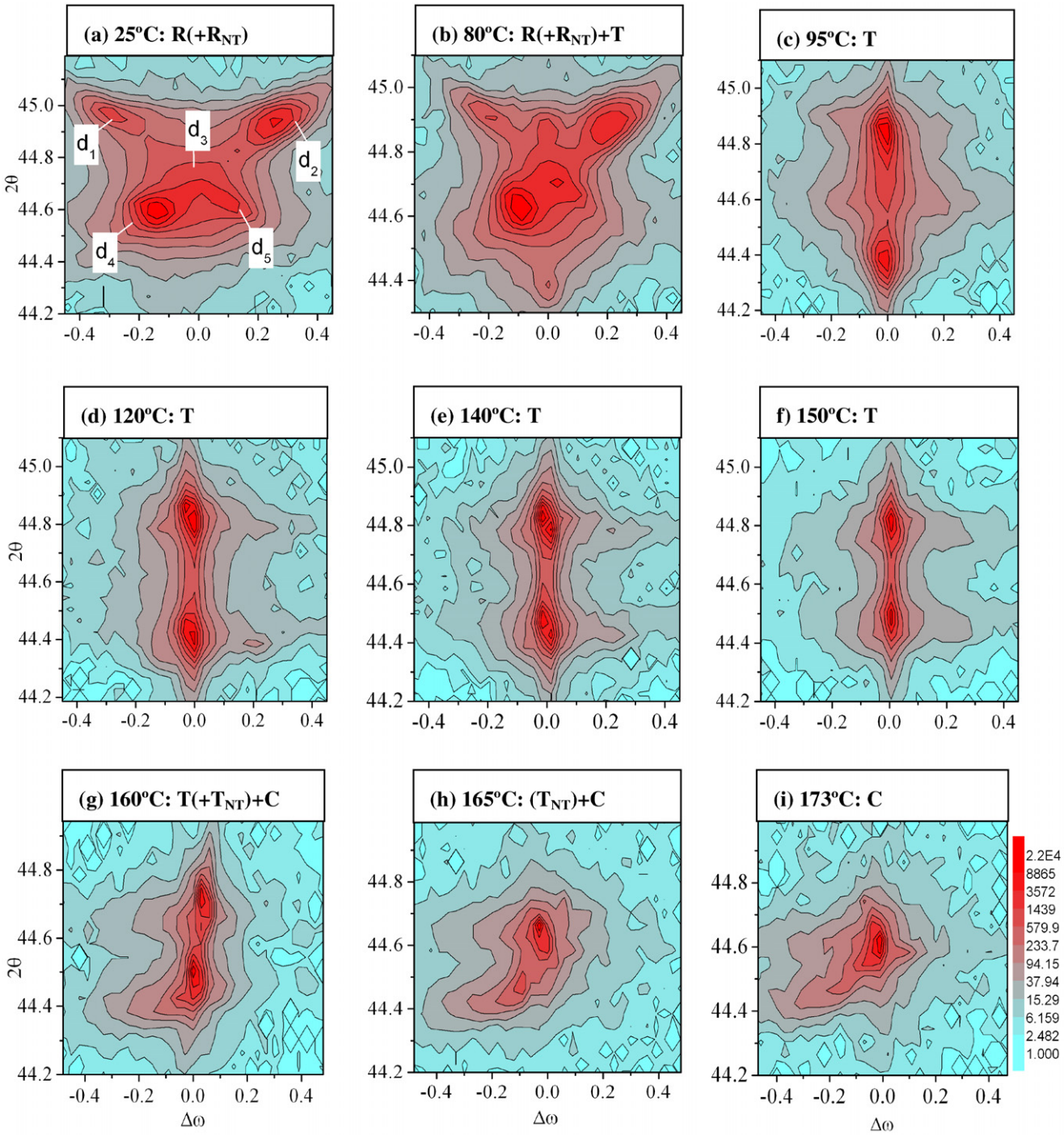

Figure 3. (002) HR-XRD mappings taken from the fractured surface of an unpoled (annealed) PZN–8%PT single crystal at (a) 25 °C, (b) 80 °C, (c) 95 °C, (d) 120 °C, (e) 140 °C, (f) 150 °C, (g) 160 °C, (h) 165 °C, and (i) 173 °C. The intensity contours are on a log scale.

E field of 0.5 kV mm^{-1} along the [001] direction. Figure 5 shows the (002) reciprocal space mappings of the poled PZN–8%PT single crystal. At 25 °C, a very broad peak, within which several barely distinguished peaks marked d_1, d_2, and d_3 in figure 5(a), could be detected. This diffraction pattern resembles that found at room temperature phase of the unpoled sample although the various diffraction peaks are not as distinct. The room temperature diffraction pattern of the poled PZN–8%PT sample is thus the same as that of the unpoled sample, save that with the various diffractions smearing out into a seemingly convoluted peak as a result of poling induced stresses in the material, as was also noted by Liu and Lynch [27]. This low-temperature phase is again referred to as the LT phase(s).

The above-described diffraction pattern remained relatively unchanged from 25 °C to about 90 °C (figure 5(b)). At 110 °C, three clear diffraction peaks emerged (figure 5(c)). The two peaks located at $2\theta \approx 44.39°$ and 44.86°, which were slightly tilted out of the $\omega = 0°$ plane, were identified as those of the T phase, while the middle peak at $2\theta \approx 44.57°$ was

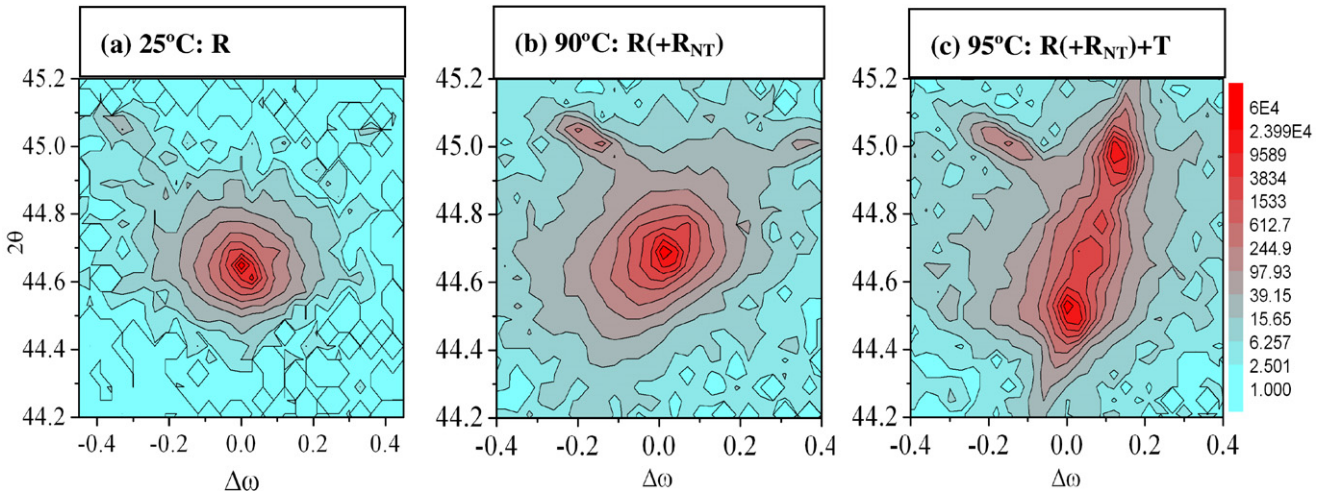

Figure 4. (002) HR-XRD mappings taken at (a) 25 °C, (b) 90 °C, and (c) 95 °C from the fractured surface of another unpoled (annealed) PZN–8%PT single crystal, illustrating slightly different diffraction patterns. The intensity contours are on a log scale.

identified to pertain to the LT phase(s). The low-temperature LT phase(s) and the T phase coexisted at 110 °C while only the T phase persisted above 115 °C. The LT phase(s) disappeared on further heating to 115 °C (figure 5(d)). Figures 5(e)–(g) show that the T phase remained the only phase detected even at 160 °C despite gradual changes in the 2θ positions with increasing temperature.

Unlike the unpoled sample, clear peak splitting became apparent at 165 °C for the poled sample. As shown in figure 5(h), five diffraction peaks could be detected which are located at largely two different Bragg's angles, i.e. d_1–d_3 at $2\theta \approx 44.76°$ and d_4 at $2\theta \approx 44.59°$. The C phase emerged shortly after and became the only phase detected at and above 170 °C (figure 5(i)).

4. Discussion

4.1. Room temperature phases of PZN–8%PT and the transformation path over 80–110 °C

The results presented in the previous section show that, at room temperature, while one unpoled PZN–8%PT displayed a diffraction pattern characteristic of the R phase (figure 4(a)), the other exhibited multiple diffraction peaks (figure 3(a)). Similarly, the poled PZN–8%PT produced a broad, possibly convoluted peak located at $2\theta \approx 44.55°$–$44.60°$ although a few degeneracy peaks are barely distinguishable in this case (figure 5(a)). The above observations suggest that at room temperature, both unpoled and poled PZN–8%PT are likely to have a microstructure which may vary from a predominantly R state to one consisting possibly of a phase mixture. The results also show that at and above 95 °C, only two peaks located at $2\theta \approx 44.37°$ and $44.86°$ were observed from both the unpoled and poled samples. These two peaks are those of the [100] and [001] diffractions of the T domains.

As mentioned above, the diffraction patterns in figures 3(a) and 5(a) may thus be assigned to either of the following two possible sources: (a) R + monoclinic (M), or (b) R (for d_3) + R_{NT} (for d_1, d_2, d_4, and d_5), where R_{NT} represents the rhombohedral phase but of nanotwin domains (as opposed to those of typical microscopic ferroelectric domains).

The following observations have led us to conclude that the diffractions at room temperature pertain to those of R(+R_{NT}). First, as shown in figure 4, another unpoled PZN–8%PT sample taken from the same wafer shows that the various degenerated peaks are not symmetrical with respect to the $\omega = 0°$ plane. More interestingly, it shows that upon heating, the asymmetrical degenerated peaks persisted and were found to coexist with the newly emerging T diffractions (figures 4(b) and (c)). Thus, the phases present over the temperature range of 110–115 °C are either R + M + T or R(+R_{NT}) + T. Other than at the eutectoid point where three phases coexist, a maximum of two phases is expected in a two-component system under equilibrium condition. This means that the LT phase cannot be a phase mixture. Hence, it must be of a single phase but of different domain configurations, i.e. it must be R(+R_{NT}). The asymmetrical degenerated peaks in figures 3(a) and 5(a) thus can be attributed to unbalanced R_{NT} domain populations in the crystal. The unbalanced domain population in the crystal has also been reported by other authors [21, 28].

It is also interesting to note that a string of current signals was detected over the temperature region of 90–113 °C (figure 2). As shown in [18], one likely cause could be the compositional segregation in the crystal, leading to a range of R(+R_{NT}) − T transformation temperatures.

In contrast to thermal current signals, the anomalies in the dielectric permittivity over the temperature range of 90–115 °C remained not obvious especially for the unpoled sample. A question arises as to why no sharp anomaly was observed in the dielectric permittivity over the said temperature range for the unpoled sample. A similar observation was made in our earlier work on unpoled (annealed) PZN-4.5%PT [18]. Despite undergoing the R–T–C phase transformation, all being of first-order, no obvious anomaly was noted in the dielectric permittivity of the unpoled PZN-4.5%PT upon heating, except at the dielectric permittivity maximum, T_{max}. This latter was attributed to the effect of the strong dynamic relaxation

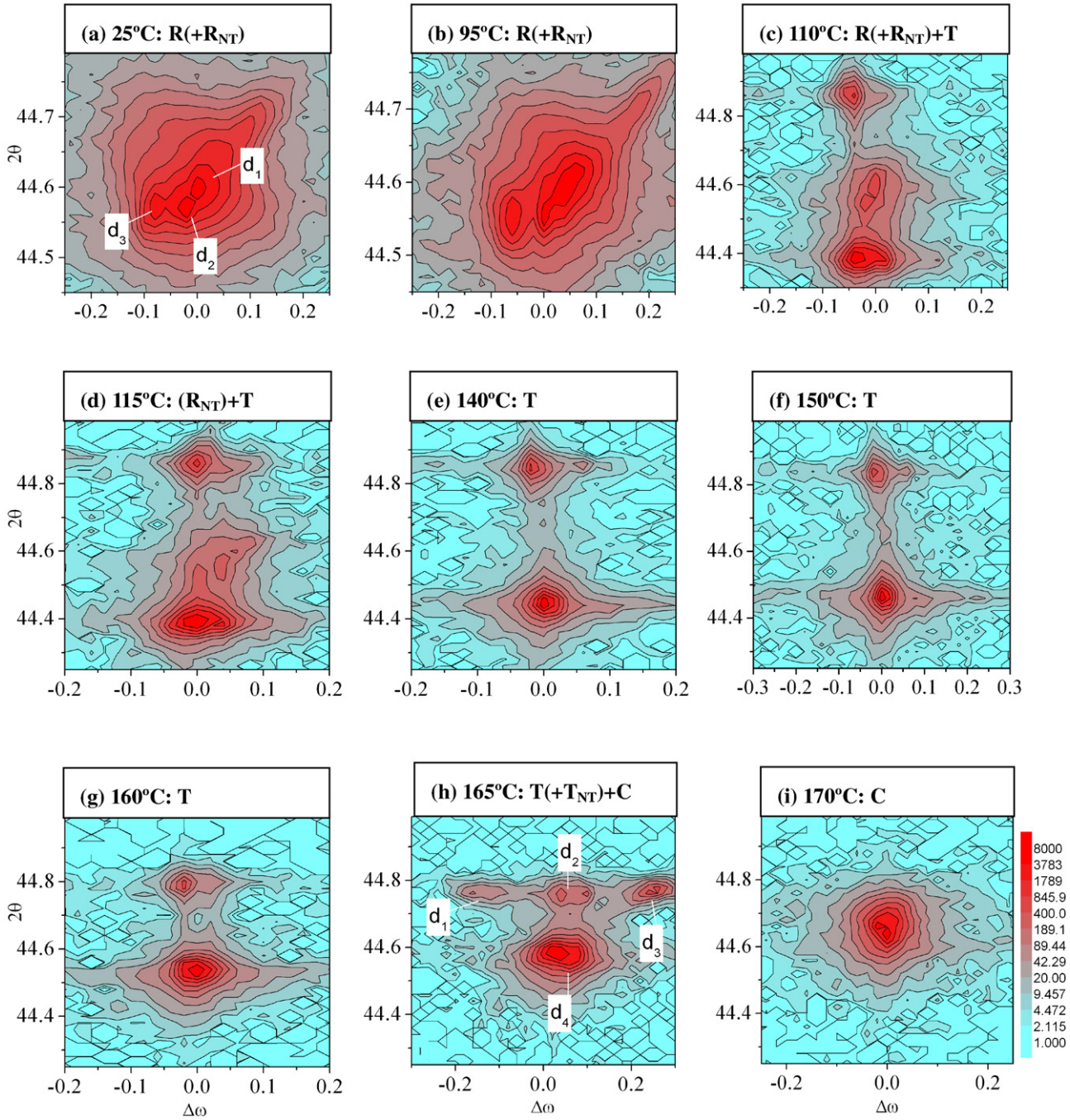

Figure 5. (002) HR-XRD mappings taken from the fractured surface of an annealed-and-poled PZN–8%PT single crystal at (a) 25 °C, (b) 95 °C, (c) 110 °C, (d) 115 °C, (e) 140 °C, (f) 150 °C, (g) 160 °C, (h) 165 °C, and (i) 170 °C. The intensity contours are on a log scale.

processes of the polar nanoclusters in the material, which help mask the anomalies in the dielectric permittivity displayed by the R–T transformation. The same is likely to occur in the unpoled PZN–8%PT sample and may explain the observations made in the present work.

4.2. Phase transformation over the temperature range of 155–170 °C

Meanwhile in the poled PZN–8%PT single crystal upon heating to 165 °C (figure 5(h)), four diffraction peaks (marked d_1 to d_4) could be distinguished. Note that except for the eutectoid point, a maximum of two phases is present in a two-component system under equilibrium conditions. Judging from figure 5, the T phase persisted to about 160 °C. Upon heating to 170 °C, the C phase was observed. Ruling out the coexistence of T + M + C phases, such a diffraction pattern over the temperature range of 165–170 °C may be assigned to either (a) T (for d_2 and d_4) + T_{NT} (for d_1 and d_3) + C (for d_4), or (b) M + C.

Should the phases present be M + C phases, at least two thermal current signals will be detected over the temperature range of 165–175 °C, corresponding to the T–M and M–C

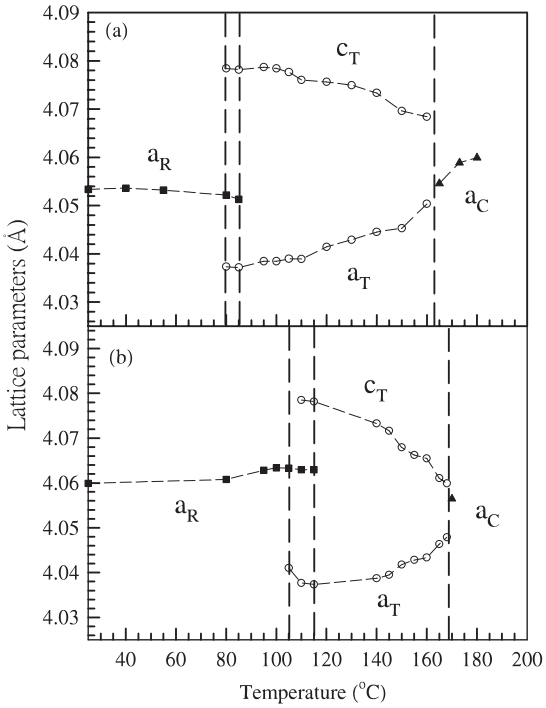

Figure 6. Temperature dependence of the lattice parameters of (a) unpoled (annealed) and (b) annealed-and-poled PZN–8%PT single crystals at the $\omega = 0°$ plane under the ZFH process, showing the phase transformation sequence of $R(+R_{NT}) - T(+T_{NT})C$.

transformations. Examination of the current signals revealed only one major current signal, which is consistent with that of the $T(+T_{NT}) - C$ transformation. We may thus conclude that the phase present at 165 °C is the mixture of $T(+T_{NT}) + C$.

The high-temperature transformation paths of both unpoled and poled PZN–8%PT single crystals are thus consistent, being $T(+T_{NT}) - C$, where the T_{NT} phase serves as a bridging phase between the T and C end phases. The anomaly in dielectric permittivity and the thermal current signals at about 160–173 °C may thus be attributed to the $T(+T_{NT}) - C$ transformation event in both the unpoled and poled samples.

The temperature dependence of lattice parameters of R, T, and C phases of both the unpoled (annealed) and annealed-and-poled PZN–8%PT at the $\omega = 0°$ plane are determined from the relevant HR-XRD reciprocal space mappings. The results are shown in figure 6.

5. Conclusions

With HR-XRD, dielectric permittivity, and thermal current density data, the present work shows that the room temperature state of both unpoled and poled PZN–8%PT single crystals is rhombohedral, consisting of a mixture of microscopic (R) and nanotwin (R_{NT}) domains. Upon heating under zero-field conditions, both the unpoled and poled PZN–8%PT eventually take the $R(+R_{NT}) - T(+T_{NT}) - C$ transformation path, the T_{NT} occurring as a brief bridging state between the T and C end phases.

Acknowledgments

The authors gratefully acknowledge the financial support received from the Ministry of Education (Singapore) and the National University of Singapore, via research grants Nos R-265-000-221-112, R-265-000-257-112, R-265-000-261-123/490, and R-265-000-257-731, support received by SSLS via NUS Core Support C-380-003-003-001, A*STAR/MOE RP 397990 8M, A*STAR 012 105 0038 grants, and from the National Science Council of Taiwan via grant No. 95-2112-M-030-001.

References

[1] Park S-E and Shrout T R 1997 *J. Appl. Phys.* **82** 1804–11
[2] Fu H and Cohen R E 2000 *Nature* **403** 281–3
[3] Bellaiche L, Garcia A and Vanderbilt D 2000 *Phys. Rev. Lett.* **84** 5427–30
[4] Vanderbilt D and Cohen M H 2001 *Phys. Rev.* B **63** 094108
[5] Noheda B, Cox D E, Shirane G, Park S-E, Cross L E and Zhong Z 2001 *Phys. Rev. Lett.* **86** 3891–4
[6] Cox D E, Noheda B and Shirane G 2001 *Appl. Phys. Lett.* **79** 400–2
[7] Noheda B, Zhong Z, Cox D E, Shirane G, Park S-E and Rehrig P 2002 *Phys. Rev.* B **65** 224101
[8] La-Orauttapong D, Noheda B, Ye Z-G, Gehring P M, Toulouse J, Cox D E and Shirane G 2002 *Phys. Rev.* B **65** 144101
[9] Noheda B 2002 *Curr. Opin. Solid State Mater. Sci.* **6** 27–34
[10] Lu Y, Jeong D-Y, Cheng Z-Y, Shrout T and Zhang Q M 2002 *Appl. Phys. Lett.* **80** 1918–20
[11] Kisi E H, Piltz R O, Forrester J S and Howard C J 2003 *J. Phys.: Condens. Matter* **15** 3631–40
[12] Viehland D 2000 *J. Appl. Phys.* **88** 4794–806
[13] Jin Y M, Wang Y U, Khachaturyan A G, Li J F and Viehland D 2003 *Phys. Rev. Lett.* **91** 197601
[14] Wang Y U 2006 *Phys. Rev.* B **74** 104109
[15] Wang Y U 2007 *Phys. Rev.* B **76** 024108
[16] Bdikin I K, Shvartsman V V and Kholkin A L 2003 *Appl. Phys. Lett.* **83** 4232–4
[17] Lim L C, Chang W S, Rajan K K, Shanthi M, Yang P, Moser H O, Tu C-S, Wang F-T, Tseng C-T, Bhalla A S and Guo R 2008 *J. Appl. Phys.* **103** 084122
[18] Chang W S, Lim L C, Yang P, Tu C-S, Wang F-T and Tseng C-T 2008 *J. Appl. Phys.* **104** 054102
[19] Wang H, Zhu J, Lu N, Bokov A A, Ye Z-G and Zhang X W 2006 *Appl. Phys. Lett.* **89** 042908
[20] Ohwada K, Hirota K, Rehrig P W, Fujii Y and Shirane G 2003 *Phys. Rev.* B **67** 094111
[21] Uesu Y, Matsuda M, Yamada Y, Fujishiro K, Cox D E, Noheda B and Shirane G 2002 *J. Phys. Soc. Japan* **71** 960–5
[22] Lim L C and Rajan K K 2004 *J. Cryst. Growth* **271** 435
[23] Chang W S, Shanthi M, Rajan K K, Lim L C, Wang F T, Tseng C T, Tu C S, Yang P and Moser H O 2007 *J. Appl. Phys.* **101** 124104
[24] Chang W S, Lim L C, Wang F-T, Tu C-S and Yang P 2008 *J. Appl. Phys.* **103** 074110
[25] Vugmeister B E and Rabitz H 1998 *Phys. Rev.* B **57** 7581–5
[26] Blinc R, Laguta V V, Zalar B and Banys J 2006 *J. Mater. Sci.* **41** 27–30
[27] Liu T and Lynch C S 2006 *Contin. Mech. Thermodyn.* **18** 119–35
[28] Kisi E H, Forrester J S, Howard C J and Ibberson R M 2007 *J. Phys.: Condens. Matter* **19** 232201